Spin-lozenge thermodynamics and magnetic excitations in Na_3RuO_4

Spin-lozenge thermodynamics and magnetic excitations in Na$_3$RuO$_4$

J T Haraldsen[1,2], **M B Stone**[3], **M D Lumsden**[3], **T Barnes**[1,4],
R Jin[1,2,5], **J W Taylor**[6] and **F Fernandez-Alonso**[6]

[1] Department of Physics and Astronomy, University of Tennessee, Knoxville, TN 37996, USA

[2] Materials Science and Technology Division, Oak Ridge National Laboratory, Oak Ridge, TN 37831, USA

[3] Neutron Scattering Science Division, Oak Ridge National Laboratory, Oak Ridge, TN 37831, USA

[4] Physics Division, Oak Ridge National Laboratory, Oak Ridge, TN 37831, USA

[5] Department of Physics and Astronomy, Louisiana State University, Baton Rouge, LA 70803, USA

[6] ISIS Facility, Rutherford Appleton Laboratory, Chilton, Didcot, Oxfordshire OX11 0QX, UK

Abstract
We report inelastic and elastic neutron scattering, magnetic susceptibility, and heat capacity measurements for polycrystalline sodium ruthenate (Na$_3$RuO$_4$). Previous work suggests that this material consists of isolated tetramers of $S = 3/2$ Ru^{5+} ions in a so-called lozenge configuration. Comparisons of magnetic susceptibility and inelastic and elastic neutron scattering results with analytic calculations for several cluster models show that although there may be significant spin–spin correlations within the lozenge cluster, a simple isolated lozenge model is not appropriate for Na$_3$RuO$_4$.

(Some figures in this article are in colour only in the electronic version)

1. Introduction

Magnetic materials have received continuous research interest in chemistry, physics, and materials science [1–4], due to their technological impact [5] and the fundamental physical phenomenon that many such materials display [6]. Perovskite-based alkali metal ruthenates have just recently gained attention [7–10]. These ruthenates exhibit a range of properties from ferro- and para-magnetism to superconductivity [11–13] and have been shown to demonstrate an interesting cross-road in condensed matter physics [14–17]. Several ruthenate compounds have also been considered as model systems of geometric frustration or low-dimensional magnetism [18–20]. Na$_3$RuO$_4$ is one such ruthenate which has been proposed to consist of isolated or weakly coupled tetramers of spins in a so-called lozenge configuration. Such a configuration of antiferromagnetically interacting quantum spins is intriguing as it is one of the simplest perturbations of the canonical frustrated antiferromagnetic equilateral spin-trimer. The value of the spin quanta in Na$_3$RuO$_4$ ($S = 3/2$) also make this compound a potential experimental frustrated system bridging between the physics of frustrated quantum ($S = 1/2$) magnets

and classical, three-dimensional, frustrated magnetic systems such as the spin-ice pyrochlores [21–23].

The structure of Na$_3$RuO$_4$ was first examined by Darriet *et al* [24]. Na$_3$RuO$_4$ consists of oxygen coordinated sodium and ruthenium sites within the *ab* plane, separated by a single layer of sodium sites displaced along the *c*-axis. The structure of Na$_3$RuO$_4$ was recently revisited and determined to be monoclinic, with space group $C2/m$ and lattice parameters $a = 11.0295(6)$ Å, $b = 12.8205(7)$ Å, $c = 5.7028(3)$ Å, and $\beta = 109.90(3)°$ [10][7]. Figure 1(a) illustrates a single plane of Ru ions together with coplanar oxygen and sodium ions. The Ru ions are octahedrally coordinated through shared oxygens and each Ru^{5+} ion may be modeled as having a local spin $S = 3/2$. This arrangement of ions suggests a local tetramer or lozenge spin configuration, as shown in figures 1(a)–(b). An isolated spin-lozenge with exchange constants $J = 3.36$ meV and $\alpha J = 3.88$ meV (see figure 1(a)) was first proposed by Drillon *et al* in order to describe magnetic susceptibility

---

[7] We believe there are two typographical errors in the table of atomic coordinates in [10]. The atomic coordinates for site Na$_3$ should be $x = 0.2421$, $y = 0.1254$ and $z = 1/2$ and site O$_3$ should be $x = 0.1528$, $y = 1/2$ and $z = 0.1969$.
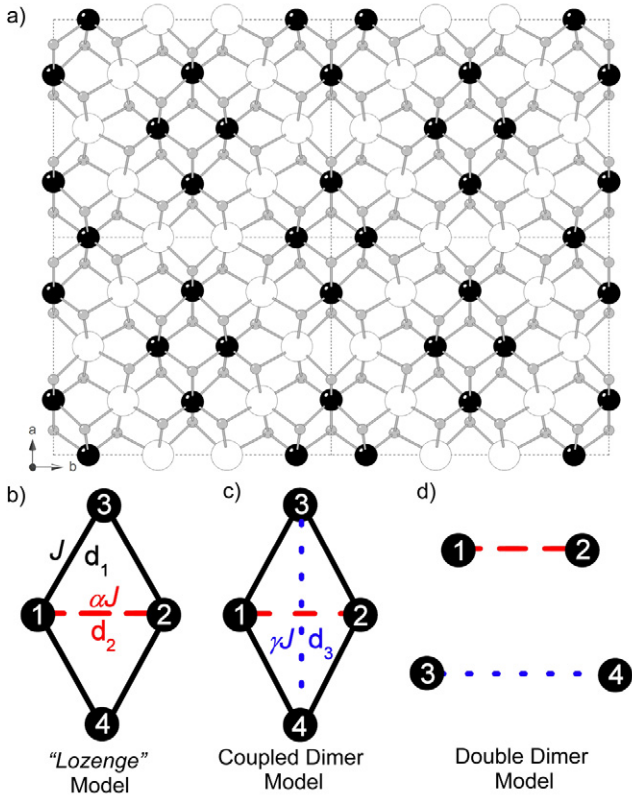
Figure 1. Crystal structure and potential exchange interaction models for Na_3RuO_4. (a) Crystal structure as viewed along the c-axis showing a single plane of atomic sites for $\pm c/4$ unit cells. Ru, O and Na sites are black, gray, and white respectively. The monoclinic $C2/m$ unit cell is shown as dashed gray lines. (b)–(d) are three possible models of exchange interactions between Ru sites in the ab plane as discussed in the text. The double dimer model is not spatially confined, and represents two individual dimers.

measurements [25]. However, the existence of long-range antiferromagnetic order below $T \approx 30$ K was established using Mossbauer spectroscopy [26], and provided the first indication that the suggestion of isolated antiferromagnetic tetramer clusters in Na_3RuO_4 may be incorrect. Recent measurements of magnetic susceptibility have also been interpreted in terms of a spin tetramer model [10]. Temperature dependent neutron diffraction studies have confirmed the existence of long-range magnetic order below $T_N \approx 30$ K. The magnetic long-range ordered phase immediately calls into question the accuracy of an isolated spin tetramer model for Na_3RuO_4.

In this paper, we present thermodynamic and inelastic and elastic neutron scattering measurements of Na_3RuO_4 quantifying the possibility of significant correlations within a dimer or tetramer spin-cluster. We find that there are in fact two subsequent magnetic phase transitions at low temperature. We also find a low energy excitation which is highly dispersive, gapless, and heavily damped in the disordered phase. However, the spectrum of magnetic excitations also exhibits features which are more localized in nature, likely due to antiferromagnetic dimers in the ab plane.

2. Experimental techniques

Powder samples of Na_3RuO_4 were prepared by solid-state reactions from stoichiometric amounts of NaOH and RuO_2. The starting stoichiometric mixture was initially ground together and then held at 500 °C for 20 h under an O_2 atmosphere. After re-grinding, the powder was heated to 650 °C for another 20 h, again under an O_2 atmosphere. The resulting dark gray powder was reground and checked for impurity phases using x-ray diffraction. If any impurity phases were evident, the powder was refired and the process repeated. This growth procedure is similar to that described in [10]. Powder refinement of room temperature x-ray diffraction measurements yielded lattice parameters of $a = 11.012(7)$, $b = 12.809(9)$, $c = 5.687(3)$ Å, and $\beta = 109.91(3)°$ for the $C2/m$ monoclinic unit cell (see footnote 7). These values compare well to the fully refined structure described in [10]. Single crystals of appropriate mass are unfortunately not yet available for inelastic neutron scattering (INS) measurements.

Heat capacity measurements were performed on a small single crystal of mass ≈ 10 mg, which was obtained through the synthesis procedure described above. This single crystal grew as a small platelet, with the c-axis normal to the plane of the platelet. Heat capacity measurements were performed with a commercial calorimeter between $T = 1.8$ and 300 K using the relaxation technique. Measurements were carried out in zero and 8 T applied magnetic fields with the field applied parallel to the c-axis.

Magnetization measurements were performed on powder and single crystal samples using a commercial SQUID magnetometer as a function of applied magnetic field and temperature. SQUID measurements performed on the same single crystal sample that was used for heat capacity measurements agree well with those performed on a powder sample.

INS measurements were performed using the MARI time-of-flight spectrometer at the ISIS neutron scattering facility [27]. This instrument allows for a rapid measure of scattering intensity over a broad portion of wavevector and energy transfer space. The sample consisted of ≈ 45 g of Na_3RuO_4 powder in a square aluminum foil sachet (approximately 50 mm × 50 mm × 8 mm), suspended from the cold-tip of a closed-cycle He^4 refrigerator. The sachet was oriented with the 50 mm × 50 mm surface normal to the incident neutron beam. An incident energy of $E_i = 25$ meV was used, and data were taken at several temperatures between $T = 8$ and 305 K. This configuration resulted in a measured instrumental full width at half maximum (FWHM) energy resolution at the elastic position of $\delta\hbar\omega = 0.982(7)$ meV. Data were corrected for detector sensitivity through room temperature measurements of a vanadium standard.

INS measurements were also made using the HB3 triple-axis spectrometer at the high flux isotope reactor (HFIR) at Oak Ridge National Laboratory. This instrument allows one to perform inelastic measurements focusing on specific portions of wavevector and energy transfer space as a function of temperature. For these measurements, the sample consisted of 20.7 g of Na_3RuO_4 powder in a cylindrical aluminum sample
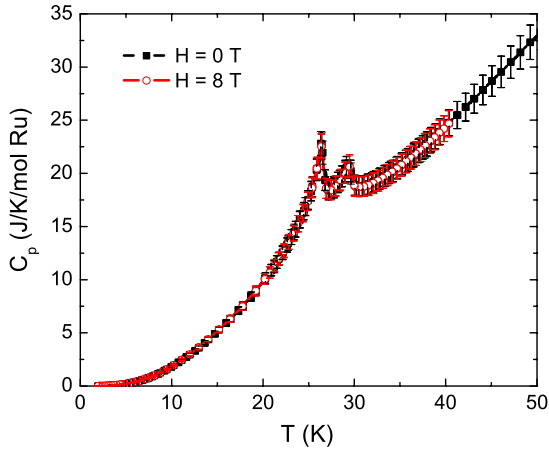
Figure 2. Heat capacity of a Na_3RuO_4 single crystal. Measurements were performed at zero field (black squares) and $H = 8$ T (red open circles), with $H \parallel c$. Error bars represent an estimated five per cent error in the measurement.
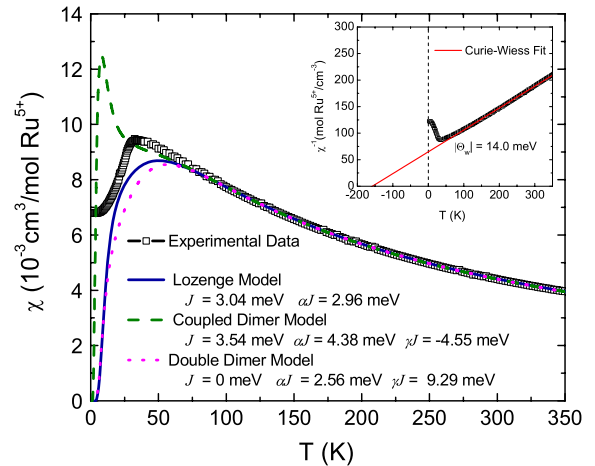

Figure 3. Magnetic susceptibility of Na_3RuO_4 powder (black squares), showing fits using the three models: Lozenge (solid blue), coupled dimer (dashed green), and double dimer (dotted magenta). The inset shows χ^{-1}, with a Curie–Weiss fit as described in the text.

can 18 mm in diameter and 57 mm tall. The sample can was sealed under He gas and mounted to the cold-tip of a closed-cycle He^4 refrigerator. Horizontal collimation was chosen as $48'$–$40'$–$40'$–$120'$ between source and monochromator, monochromator and sample, sample and analyzer, and analyzer and detector, respectively. The spectrometer was operated with fixed final energy, $E_f = 14.7$ meV, using a pyrolytic graphite (PG 002) monochromator and analyzer. Pyrolytic graphite filters were placed between the sample and analyzer to reduce higher-order spurious scattering processes. In this configuration, the energy resolution at the elastic position was $\delta\hbar\omega = 1.10(2)$ meV FWHM, as measured from the incoherent scattering at $Q = 1.2$ Å^{-1}. The wavevector resolution was measured to be $\delta Q = 0.0407(7)$ Å^{-1} FWHM using the (110) nuclear Bragg peak. All measurements were made per fixed incident neutron monitor count.

Elastic neutron scattering measurements were also performed using the HB3 triple-axis spectrometer, with $E_i = E_f = 14.7$ meV. These measurements were performed on the same powder sample as the inelastic HB3 measurements, with horizontal collimation $48'$–$20'$–$20'$–$70'$. This resulted in an energy resolution at the elastic position of $\delta\hbar\omega \approx 0.8$ meV FWHM. The wavevector resolution was measured to be $\delta Q = 0.0254(9)$ Å^{-1} FWHM using the (110) nuclear Bragg peak.

INS measurements were also performed to place limits on the value of a possible energy gap in the excitation spectrum. These were performed using the IRIS backscattering spectrometer at the ISIS neutron source at the Rutherford Appleton Laboratory [28]. The IRIS spectrometer allows one to measure excitations at small energy transfers with very good energy resolution. It also allows one to simultaneously obtain a high resolution neutron diffraction pattern. The sample measured was the identical powder used for the HB3 measurements. The IRIS spectrometer was operated at 25 Hz with cooled PG002 analyzers ($T = 10$ K) and a Beryllium filter ($T = 25$ K) to avoid contamination from higher-order reflections, resulting in a 17.5 μeV FWHM energy resolution at the elastic position as measured with a vanadium standard.

The high resolution (backscattering) diffraction banks with a resolution of $\Delta Q/Q = 2.5 \times 10^{-3}$ were also used.

3. Experimental results

Figure 2 shows heat capacity as a function of temperature for $H = 0$ and 8 T. There are two clear lambda-like anomalies at $T_{N1} \approx 25$ and $T_{N2} \approx 28$ K, signifying phase transitions at these temperatures. Previous neutron diffraction measurements have shown the existence of only a single, broad phase transition near 30 K corresponding to the onset of long-range magnetic order [10]. Our heat capacity measurements indicate that the observed broad transition is likely due to two successive magnetic transitions. No change in these transition temperatures is observed for measurements at $H = 8$ T.

The magnetic susceptibility of Na_3RuO_4 was measured over the range $2 \leqslant T \leqslant 350$ K; the resulting data is shown in figure 3. Comparison to a Curie–Weiss model yields the Weiss temperature $|\Theta_W| = 14.0$ meV as illustrated in the inset of figure 3. The negative intercept in $\chi^{-1}(T)$ and the decrease in $\chi(T)$ below the transition temperature are consistent with predominant antiferromagnetic interactions.

Figure 4 shows temperature dependent INS data. At $T = 8$ K there is significant inelastic scattering intensity in the vicinity of $\hbar\omega \approx 5$ meV, which decreases in intensity rapidly with increasing wavevector, implying magnetic scattering. In the $T = 8$ K data, a weak excitation near $\hbar\omega \approx 10$ meV is also evident. There are also clear dispersing excitations propagating out of $|\mathbf{Q}| \approx 1$ Å^{-1}. As temperature increases, the inelastic scattering intensity rapidly decreases and moves to smaller wavevectors, consistent with an evolution from antiferromagnetic spin-waves to para-magnetic scattering with increasing temperature. Phonon scattering was observed at larger wavevectors and at larger energy transfers. The 18 meV excitation in figure 5 is one such phonon mode; this mode is not clearly seen in the MARI data due to kinematic constraints at large energy transfers.
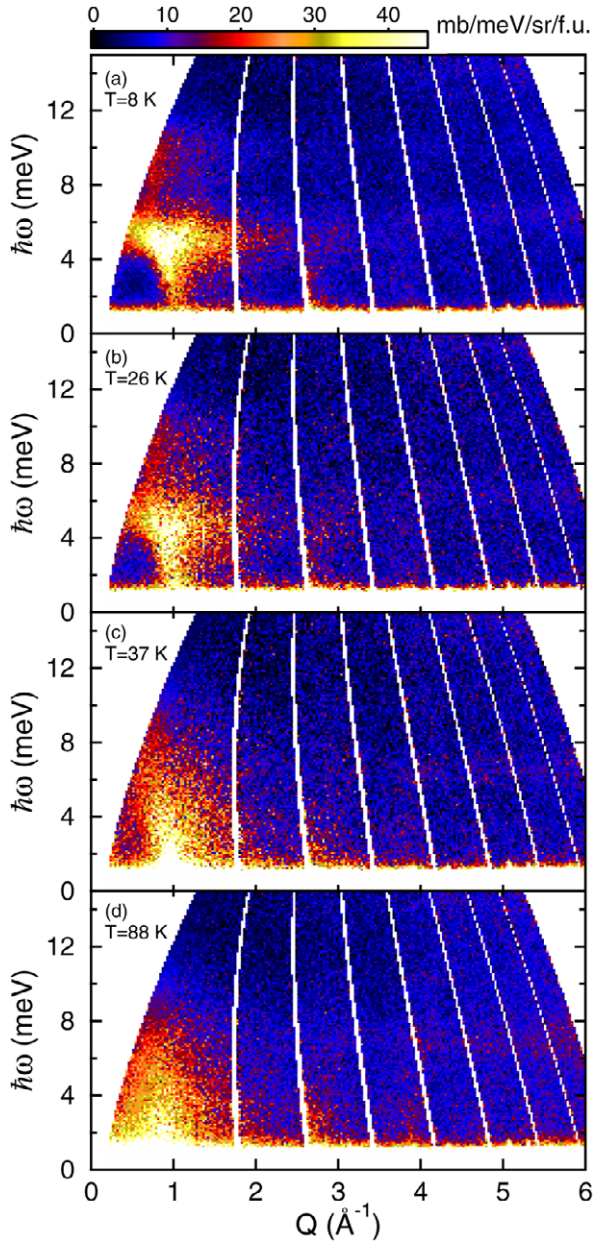
Figure 4. INS intensity from Na_3RuO_4 powder versus energy and momentum transfer at (a) $T = 8$ K, (b) $T = 26$ K, (c) $T = 37$ K and (d) $T = 88$ K. These measurements were carried out on the MARI spectrometer at an incident energy of $E_i = 25$ meV.

Figure 5. INS intensity from Na_3RuO_4 powder versus energy transfer at (a) $Q = 1.6$ Å^{-1} at $T = 8$ and 250 K and (b) integrated between 0.4 Å$^{-1} < Q < 1.6$ Å^{-1} at $T = 8$, 30 and 88 K. Black lines are Lorentzian fits, as described in the text. The data in (a) are from HB3, and the data in (b) are from MARI.

In figure 5, we show the scattering intensity as a function of energy transfer for $Q = 1.6$ Å^{-1}, measured on the HB3 spectrometer, and the integrated scattering intensity for 0.4 Å$^{-1} < Q < 1.7$ Å^{-1}, measured on the MARI spectrometer. Single Lorentzian fits to the low temperature data describe modes at $\hbar\omega = 5.03 \pm 0.08$, 9.8 ± 0.2 and 17.9 ± 0.3 meV for the data shown in figure 5(a), and $\hbar\omega = 4.95 \pm 0.04$ and 9.8 ± 0.1 meV for the data shown in figure 5(b). The increase in intensity of the 18 meV excitation with increasing temperatures and wavevector dependence observed in the HB3 data suggests that this mode is a phonon.

We also examined the temperature dependence of the elastic scattering in the vicinity of $Q \approx 1$ Å^{-1}. Figure 6 shows
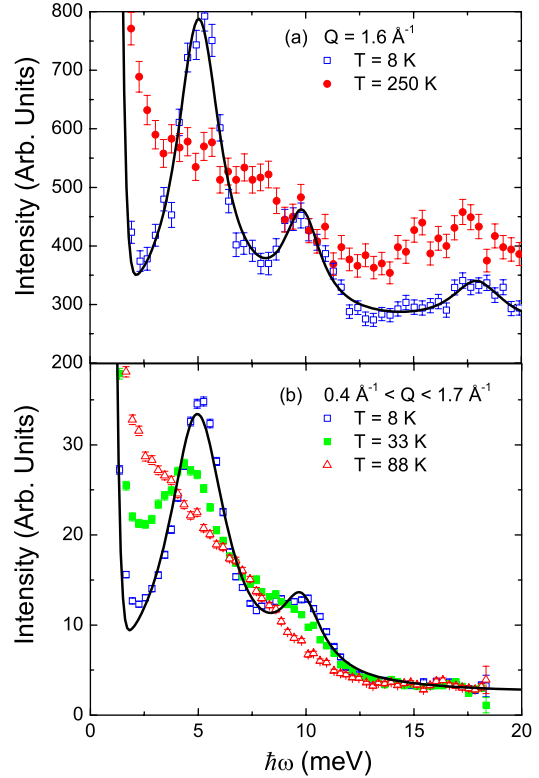
the scattering intensity observed in the HB3 Na_3RuO_4 powder measurement as a function of temperature and wavevector. As temperature is decreased, there is an increase in scattering intensity at $Q \approx 0.99$ and ≈ 1.07 Å^{-1} corresponding to the transition to long-range magnetic ordering. Note that $Q \approx 0.985$ Å^{-1} is the location of a nuclear Bragg peak. Below $T \approx 25$ K, the magnetic Bragg peaks appear to shift location as a function of decreasing temperature. The heat capacity indicates two phase transitions at $T \approx 25$ and ≈ 30 K respectively. The lower temperature phase transition is a magnetic phase transition. The $T \approx 30$ K feature is potentially a structural phase transition, and needs to be verified with higher resolution neutron scattering measurements.

High resolution backscattering measurements investigated the magnetic spectrum for energy transfers below 1.7 meV with $T = 15$ K (shown in figure 7(a)). Excitations clearly propagate out of the magnetic wavevector $Q \approx 1.1$ Å^{-1}. Figure 7(b) shows the difference of the elastic scattering intensity between the disordered and ordered phases as measured using IRIS and HB3. These data illustrate that the excitations are dispersing directly out of the magnetic Bragg peaks. The data in figures 7(a) show no indication of a gap in the magnetic spectrum down to ~ 250 μeV. Additional magnetic Bragg peaks are shown in figure 7(c), however a full refinement of the magnetic structure(s) as a function of temperature will require additional high resolution measurements over a larger range of wavevector transfer.
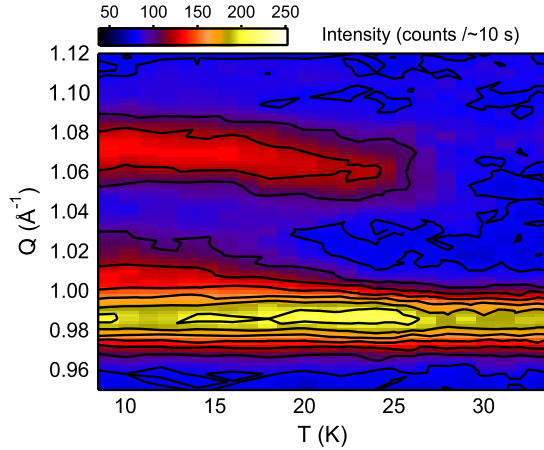
Figure 6. Elastic scattering intensity of Na_3RuO_4 as function of momentum transfer and temperature. Data were acquired using the HB3 spectrometer. The contour lines correspond to intervals of 20 counts per ten seconds, and are only plotted for count rates between 80 and 200 counts per ten seconds. The data were obtained at 20 temperatures between $T = 8.5$ and 34 K.

4. Discussion

The fact that we observe both a phase transition to long-range magnetic order as well as a highly dispersive low energy excitation immediately eliminates a purely isolated cluster model for Na_3RuO_4. However, the gradual turn-over in the temperature dependent magnetic susceptibility in the vicinity of $T = 40$ K and the weakly dispersive mode at approximately 10 meV do indicate the possible existence of finite clusters of correlated moments at finite temperature. We examine the possibility of specific cluster models consistent with the tetramer structure for both the INS and magnetic susceptibility data. Figures 1(b)–(d) show the individual configurations of the coupled dimer models we examine. In the isolated tetramer case, i.e. the lozenge model, four Ru^{5+} ions have super-exchange interactions through Ru–O–Ru bonds with bond lengths $d_1 = 3.20$, $d_2 = 3.20$, and $d_3 = 5.56$ Å, as illustrated in figure 1 [10]. A more general case of the lozenge model includes a non-zero exchange interaction γJ resulting in the coupled dimer configuration, figure 1(c). In the limit of αJ and $\gamma J \gg J$, one recovers two isolated dimers or a double dimer configuration, cf figure 1(d). We note that the double dimer model is not spatially confined to the four Ru^{5+} ions as in the lozenge configuration, but could represent other dimer interactions in the structure. Using the coupled dimer model Hamiltonian, we determine the eigenstates for general S and calculate the corresponding magnetic susceptibility for fitting purposes. Then, with the choice of the appropriate magnetic ground state, the excitations observed with INS and their corresponding structure factors are also determined.

Using nearest neighbor Heisenberg interactions and a Zeeman magnetic field term for magnetic fields **B** defining the z-axis, all three of the magnetic configurations in figure 1 can be described by a single Hamiltonian:

$$\mathcal{H} = J[(\vec{S}_1 \cdot \vec{S}_3 + \vec{S}_1 \cdot \vec{S}_4 + \vec{S}_2 \cdot \vec{S}_3 + \vec{S}_2 \cdot \vec{S}_4) \\ + \alpha \vec{S}_1 \cdot \vec{S}_2 + \gamma \vec{S}_3 \cdot \vec{S}_4] - (S_1^z + S_2^z + S_3^z + S_4^z) g\mu_B B, \quad (1)$$
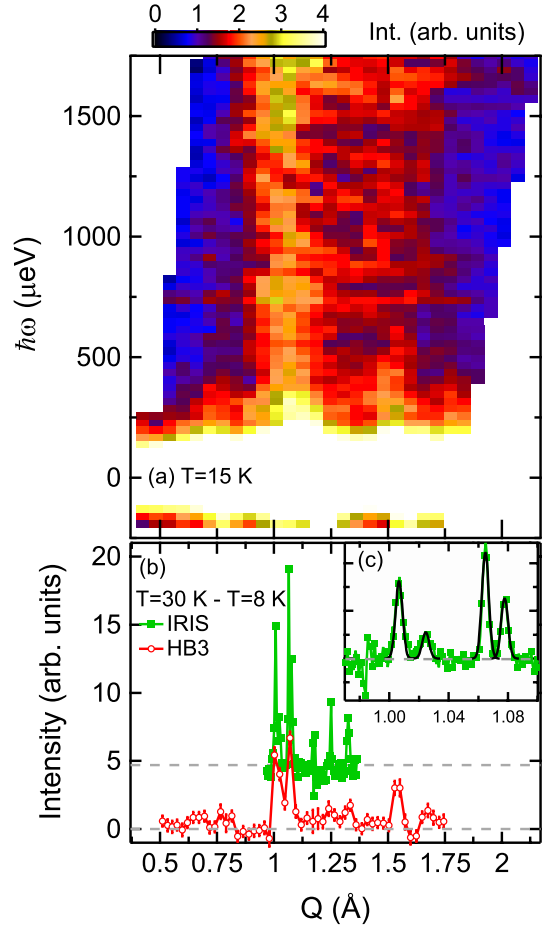

Figure 7. (a) $T = 15$ K Powder INS scattering intensity from Na_3RuO_4 as a function of energy and wavevector transfer measured using the IRIS spectrometer at ISIS. (b) Intensity as a function of wavevector transfer for data acquired at both IRIS and HB3. Data are the difference of $T = 30$ and 8 K measurements. IRIS data were acquired using the high resolution diffraction banks. HB3 data were acquired in same configuration as figure 6. Both data sets indicate clear peaks at 1.0 and 1.07 Å^{-1}. Panel (c) shows the high resolution IRIS data fitted to a series of single width Gaussian peaks at $Q = 1.006(1)$, $1.025(4)$, $1.065(1)$ and $1.078(1)$ Å^{-1}.

where αJ is the interaction for the α-dimer, γJ is the interaction for the γ-dimer, and μ_B is the Bohr magneton. We define the exchange interaction as positive for antiferromagnetic interactions, and $\vec{S}_i$ is the quantum spin operator for a spin-S ion at site $i = 1, 2, 3, 4$. By expanding the Kambe approach [2, 29], we rewrite the Hamiltonian in terms of total spin for the individual diagonalizable components, in which the eigenstates and eigenvalues of the Hamiltonian may be found by diagonalization in the convenient basis of two dimers. The energy levels are then determined simply by considering a dimer basis, where S_α corresponds to the spin state of the α dimer and S_γ corresponds to the spin state of a γ dimer as described in the Hamiltonian, equation (1). Using this dimer basis, the energy levels for the general S coupled dimer are given by

$$E = \frac{J}{2}[\mathscr{S}_{tot} + \mathscr{S}_\alpha(\alpha - 1) + \mathscr{S}_\gamma(\gamma - 1) - 2(\alpha + \gamma)\mathscr{S}] \quad (2)$$

where $\mathscr{S}_{tot} = S_{tot}(S_{tot}+1)$ with S_{tot} denoting the magnetic state of the system, $\mathscr{S}_\alpha = S_\alpha(S_\alpha + 1)$ and S_α is the spin state of the α dimer (S_1–S_2 dimer), $\mathscr{S}_\gamma = S_\gamma(S_\gamma + 1)$ and S_γ is the spin state of the γ dimer (S_3–S_4 dimer), and $\mathscr{S} = S(S + 1)$ with S being the spin of the system. The ground state of the $S = 3/2$ tetramer can either have a non-magnetic $S = 0$ ground state or a magnetic $S = 1$ ground state depending upon the values of α and γ. Simple examination of the energy levels in equation (2) indicates that, assuming antiferromagnetic exchange for J, the ground state will be non-magnetic when both α and γ are less than 4/3.

The high temperature magnetic susceptibility data were fit using the three finite cluster models for $T > 30$ K [32]. As shown in figure 3, all three cluster models qualitatively reproduce the high temperature susceptibility data. The determined exchange constants are listed in figure 3 for the three models considered. The values are consistent with predominant antiferromagnetic exchange for each of the models.

We also calculate the excitation energies and structure factors for the observable transitions of the coupled dimer models shown in figures 1(b)–(d). Such excitations would be non-dispersive in the absence of inter-tetramer exchange. For rotationally invariant magnetic interactions and an $S_{tot} = 0$ ground state in the $T = 0$ limit, only $S_{tot} = 1$ final states are observable via INS. However, due to the nature of the tetramer states being composed of dimer states, it is only possible to excite transitions of individual dimers which comprise the tetramer, $\Delta S_{\alpha/\gamma} = \pm 1, 0$. With respect to the spin-3/2 lozenge model, the values of the magnetic interactions quoted in the literature suggest a $S_{tot} = 0$ ground state, with dimer spins $S_\alpha = 3$ and $S_\gamma = 3$ [10, 25]. Therefore, due to this selective restriction of the spin excitations, only three of the nine $S_{tot} = 1$ states are accessible from that ground state through INS. The respective excitation energies ($E_{S_{tot},S_\alpha,S_\gamma}$) are

$$E_{0,3,3\rightarrow1,3,3} = J,$$
$$E_{0,3,3\rightarrow1,3,2} = J(4 - 3\gamma), \qquad (3)$$
$$E_{0,3,3\rightarrow1,2,3} = J(4 - 3\alpha),$$

and the energy-integrated powder average INS structure factors ($\bar{S}(q)_{S_{tot},S_\alpha,S_\gamma}$) for these transitions are

$$\bar{S}(q)_{0,3,3\rightarrow1,3,3} = 2|F(\vec{q})|^2(2-4j_0(qd_1)+j_0(qd_2)+j_0(qd_3)),$$
$$\bar{S}(q)_{0,3,3\rightarrow1,3,2} = \frac{|F(\vec{q})|^2}{2}(1 - j_0(qd_3)),$$
$$\bar{S}(q)_{0,3,3\rightarrow1,2,3} = \frac{|F(\vec{q})|^2}{2}(1 - j_0(qd_2)),$$
$$(4)$$

where d_1, d_2, and d_3 are the interatomic separations (shown in figure 1), $j_0(x) = \sin(x)/x$, and $|F(\vec{q})|$ is the Ru^{5+} magnetic form factor (a parameterization is given by Parkinson *et al* [30, 31]). The transition of $|00 >_{3,3}\rightarrow |1S_{tot}^z >_{3,3}$ is an excitation of the full tetramer, while the other two transitions are excitations of individual dimers.

We clearly observe two magnetic excitations at 5.0 and 9.8 meV, see figure 5. We do not find any evidence for a higher
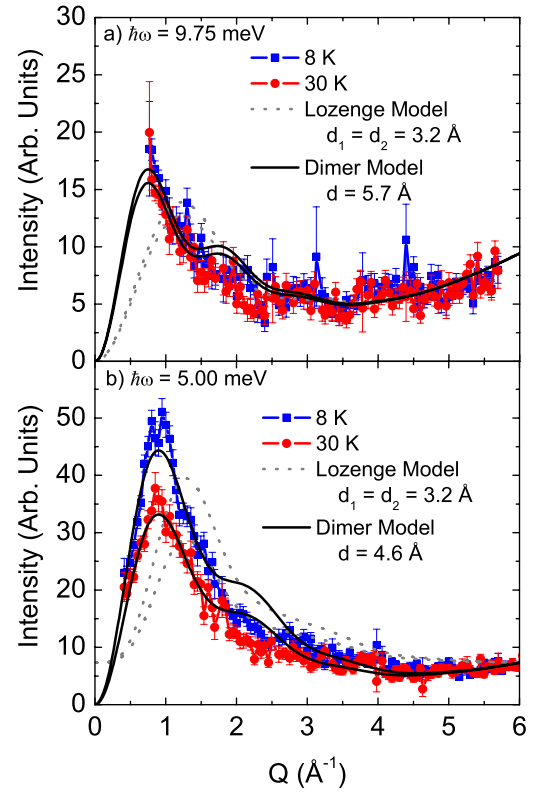

Figure 8. (a) INS intensity versus momentum transfer of the 9.8 meV excitation in Na_3RuO_4 at $T = 8$ K(blue squares) and 30 K (red circles). (b) INS intensity versus momentum transfer at $T = 8$ (blue squares) and 30 K (red circles) for the 5.0 meV excitation. Data were acquired using the MARI spectrometer as described in the text. The dotted gray lines are lozenge model fits with fixed Ru–Ru distance of 3.2 Å. The solid black lines are the double dimer model fits, where the inter-ionic distance was allowed to vary ($d = 5.7$ (a), 4.6 (b) Å).

energy excitation. Albeit, a higher energy magnetic excitation would be difficult to observe due to kinematic constraints at higher energy transfer and low wavevector transfer. Using the exchange values determined from the magnetic susceptibility the three models predict INS observable modes at 3.04, 3.28, and 12.16 meV for the lozenge model, 1.27, 3.54, and 27.80 meV for the coupled dimer model, and 2.56 and 9.29 meV for the double dimer model. Inter-cluster interactions are strong enough to result in long-range magnetic order such that the errors associated with these predicted modes may be significant. However, the double dimer model is the most reasonable simply based upon number of modes and their relative location.

Figure 8 shows constant energy scans performed above and below T_N at 5.0 and 9.8 meV energy transfer. For comparison, we fit to the calculated wavevector dependence using equation (4) for the lozenge model geometry (literature prediction) including a quadratic wavevector dependence to account for phonon scattering at larger wavevectors and an overall constant background. These lineshapes are unable to account for the initial rapid rise in scattering intensity at small wavevectors, implying significant exchange interactions between spins at larger separations than present in the lozenge model.

If the ionic distances are allowed to vary freely in fitting the data, an interesting result emerges. For the 9.8 meV excitation, the fitted separation in a single dimer model is a 5.66 ± 0.10 Å bond. This is similar to the γ-dimer length as shown in figure 1 ($d_3 = 5.56$ Å) as well as the nearest neighbor Ru–Ru distances between individual tetramers: 5.531 and 5.477 Å. Because the lower energy excitation is highly dispersive it is not clear what energy range is appropriate for modeling the scattering intensity to a isolated dimer model. Simply allowing the dimer separation to vary for the 5.0 meV data a dimer model gives a length of 4.60 ± 0.02 Å which does not correspond to any Ru–Ru separation in the structure of Na_3RuO_4.

The thermodynamic and spectroscopic evidence do not support a lozenge cluster or other cluster model as being appropriate for Na_3RuO_4. We do find that the structure factor of the 9.8 meV magnetic excitation agrees with the proposed γ-dimer shown in figure 1. However, this particular length scale is very similar to the inter-tetramer distances within the *ab* plane and even the distance between tetramer planes along the *c*-axis (5.703 Å). It is likely that this length scale of spin correlations ultimately leads to the three-dimensional ordering in Na_3RuO_4.

5. Conclusions

Considering the magnetic susceptibility and INS data and comparing these results to several tetramer models, we find that Na_3RuO_4 is not describable as a spin-lozenge or other finite tetramer model. Rather the excitations observed below T_N are likely the acoustic and optical spin-waves associated with the long-range ordered phase(s). The spin excitations in Na_3RuO_4 are very similar to those measured in the copper tellurate compounds $Cu_2Te_2O_5Cl_2$ and $Cu_2Te_2O_5Br_2$ [33]. These systems are proposed to consist of coupled $S = 1/2$ spin tetrahedra that ultimately order at low temperatures [34, 35]. INS measurements of these compounds show a single excitation which appears weakly dispersive at most wavevectors, and also like Na_3RuO_4 a dispersive spin-wave propagates out of the ordering wavevector. The Br version of the copper tellurates is thought to be more weakly coupled than the Cl compound [36] resulting in greater intra-cluster correlations above the ordering temperature, and little damping of the excitation with increasing temperature [33]. In Na_3RuO_4, like the Cl copper tellurate, we find that the excitations are highly damped with increasing temperature as shown in figure 5, indicating significant inter-tetramer coupling.

The similarity of the fundamental properties and detailed excitation spectrum of these two systems is suggestive of universal behavior in tetramer spin systems. Further single crystal diffraction and inelastic measurements will help to explore the commonalities of this material to the copper tellurates. Exploring the properties and magnetic excitations in other tetramer systems such as $Cu_4Te_5O_{12}Cl_4$ [37, 38] or $Na_5RbCu_4(AsO_4)_4Cl_2$ [39] will help to further understand the universality of these properties.

We also note that heat capacity and elastic neutron scattering measurements show that there are two distinct magnetic phase transitions in this material, at $T \approx 23$ and 28 K. This is the first evidence for two low temperature phase transitions in this material. Clearly, an understanding the nature of these long-range ordered magnetic phases will provide useful additional information regarding the nature of the magnetic interactions in Na_3RuO_4. We anticipate neutron diffraction measurements on single crystal samples of Na_3RuO_4 will be the most useful next step in the studies of this material. An interpretation of significant magnetic exchange based upon a determined ordered magnetic structure and electronic structure [40] would serve to further define the nature of the exchange coupling in Na_3RuO_4.

Acknowledgments

References

[1] Heisenberg W 1926 *Z. Phys.* **38** 411
[2] Gatteschi D, Sessoli R and Villain J *Molecular Nanomagnets* (Oxford: Oxford University Press)
[3] Dagotto E and Rice T M 1996 *Science* **271** 618
[4] Kahn O 1993 *Molecular Magnetism* (New York: VCH)
[5] Nielsen M A and Chuang I L 2000 *Quantum Computation and Quantum Information* (Cambridge: Cambridge University Press)
[6] Barra A L, Caneschi A, Cornia A, Frabrizide de Biani F, Gatteschi D, Sangregorio C, Sessoli R and Sorace L 1999 *J. Am. Chem. Soc.* **121** 5302
[7] Shaplygin I S and Lazarev V B 1980 *Russ. J. Inorg. Chem.* **25** 1837
[8] Shikano M, Delmas C and Darriet J 2004 *Inorg. Chem.* **43** 1214
[9] Shikano M, Kremer R K, Ahrens M, Koo H-J, Whangbo M-H and Darriet J 2004 *Inorg. Chem.* **43** 5
[10] Regan K A, Huang Q and Cava R J 2005 *J. Solid State Chem.* **178** 2104
[11] Callaghan A, Moeller C W and Ward R 1966 *Inorg. Chem.* **5** 1572
[12] Rijssenbeek J T, Jin R, Zadorozhny Y, Liu Y, Batlogg B and Cava R J 1999 *Phys. Rev. B* **59** 4561
[13] Maeno Y, Hashimoto H, Yoshida K, Hishizaki S, Fujita T, Bernorz J G and Lichtenberg F 1994 *Nature* **372** 532
[14] Cava R J 2004 *J. Chem. Soc. Dalton Trans.* **19** 2979
[15] Regan K A, Huang Q, Lee M, Ramirez A P and Cava R J 2006 *J. Solid State Chem.* **179** 195
[16] Alexander A, Battle P D, Burley J C, Gallon D J, Grey C P and Kim S H 2003 *J. Mater. Chem.* **10** 2612
[17] Mogare K M, Friese K, Klein W and Jansen M 2004 *Z. Anorg. Allg. Chem.* **630** 547
[18] Mao Z Q, He T, Rosario M M, Nelson K D, Okuno D, Ueland B, Deac I G, Schiffer P, Liu Y and Cava R J 2003 *Phys. Rev. Lett.* **90** 186601
[19] Soma M and Sato H 2006 *J. Phys. Soc. Japan* **75** 124802

[20] Bae J S, Yang I-S, Lee S, Noh T W, Takeda T and
Kanno R 2006 *Phys. Rev.* B **73** 052301
[21] Snyder J, Slusky J S, Cava R J and Schiffer P 2001 *Nature*
413 48
[22] Bramwell S T, Harris M J, den Hertog B C, Gingras M J P,
Gardner J S, McMorrow D F, Wildes A R, Cornelius A L,
Champion J D M, Melko R G and Fennell T 2001 *Phys. Rev.
Lett.* **87** 047205
[23] Kadowaki H, Ishii Y, Matsuhira K and Hinatsu Y 2002 *Phys.
Rev.* B **65** 144421
[24] Darriet J and Galy J 1974 *Bull. Soc. Fr. Mineral. Crystallogr.*
97 3
[25] Drillon M, Darriet J and Georges R 1977 *J. Phys. Chem. Solids*
38 411
[26] Gibb T C, Greatrex R and Greenwood N N 1980 *J. Solid State
Chem.* **31** 153
[27] Arai M, Taylor A D, Bennington S M and Bowden Z A 1992
Recent Developments in the Physics of Fluids
ed W S Howells and A K Soper (Bristol: Hilger) p F291
[28] Carlile C J and Adams M A 1992 *Physica* B **182** 431
[29] Kambe K 1950 *J. Phys. Soc. Japan* **5** 48
[30] Parkinson N G, Hatton P D, Howard J A K, Ritter C,
Chiend F Z and Wue M-K 2003 *J. Mater. Chem.* **13** 1468

[31] Parkinson N G, Hatton P D, Howard J A K, Giblin S R, Terry I,
Ritter C, Moke B-H and Wue M-K 2005 *J. Mater. Chem.*
15 1375
[32] Haraldsen J 2008 Nanomagnets: magnetic properties and
inelastic neutron scattering studies *PhD Thesis* University of
Tennessee
[33] Crowe S J, Majumdar S, Lees M R, Paul D McK, Bewley R I,
Levett S J and Ritter C 2005 *Phys. Rev.* B **71** 224430
[34] Johnsson M, Turnroos K W, Mila F and Millet P 2000 *Chem.
Mater.* **12** 2853
[35] Zaharko O, Daoud-Aladine A, Streule S, Mesot J,
Brown P-J and Berger H 2004 *Phys. Rev. Lett.* **93** 217206
[36] Lemmens P, Choi K-Y, Kaul E E, Geibel C, Becker K,
Brenig W, Valenti R, Gros C, Johnsson M, Millet P and
Mila F 2001 *Phys. Rev. Lett.* **87** 227201
[37] Takagi R, Johnsson M, Gnezdilov V, Kremer R K,
Brenig W and Lemmens P 2006 *Phys. Rev.* B **74** 014413
[38] Rahaman B, Jeschke H O, Valenti R and Saha-Dasgupta T 2007
Phys. Rev. B **75** 024404
[39] Clayhold J A, Ulutagay-Kartin M, Hwu S-J, Koo H-J,
Whangbo M-H, Voigt A and Eaiprasertsak K 2002 *Phys.
Rev.* B **66** 052403
[40] Whangbo M-H, Koo H-J, Dai D and Jung D 2003 *Inorg. Chem.*
42 3898